Investigation of microstructure within metal welds by energy resolved neutron imaging

Investigation of microstructure within metal welds by energy resolved neutron imaging

A S Tremsin[1*], W Kockelmann[2], A M Paradowska[3], Shu-Yan Zhang[2], A M Korsunsky[4], T Shinohara[5], W B Feller[6], E H Lehmann[7]

[1] University of California at Berkeley, Berkeley, CA 94720, USA
[2] STFC, Rutherford Appleton Laboratory, ISIS Facility, Didcot, OX11 0QX, UK
[3] Australian Nuclear Science and Technology Organization, Lucas Heights, NSW 2232, Australia
[4] Department of Engineering Science, University of Oxford, Oxford OX1 3PJ, UK
[5] Japan Atomic Energy Agency, 2-4 Shirakata-shirane Tokai-mura, Naka-gun Ibaraki 319-1195, Japan
[6] NOVA Scientific, Inc., 10 Picker Rd., Sturbridge, MA 01566, USA
[7] Paul Scherrer Institute, CH-5232 Villigen, Switzerland

E-mail: ast@ssl.berkeley.edu

Abstract. The recent development of bright pulsed neutron sources and high resolution neutron counting detectors enables simultaneous acquisition of a neutron transmission spectrum for each pixel of the image. These spectra can be used to reconstruct microstructure parameters within welds, such as strain, texture and phase composition through Bragg edge analysis, and in some cases elemental composition through resonance absorption analysis. In this paper we demonstrate the potential of energy-resolved neutron imaging to study the microstructures of two steel welds, where the spatial distribution of residual strain within the welds, as well as some information on the texture, are obtained with sub-mm spatial resolution. A friction stir weld of two steel plates and a conventional weld of two steel pipes were studied at pulsed neutron facilities, where a $\Delta\lambda/\lambda$ resolution as low as 0.2% can be attained over a wide range of neutron wavelengths ranging from 0.5 Å to 8 Å.

1. Introduction

A number of techniques to study the microstructures within metal welds with sub-mm spatial resolution have been developed to date. Neutron imaging is a rather unconventional method due to the fact that studies can only be performed at a limited number of bright neutron sources. However, the high degree of neutron penetration can provide a unique opportunity to investigate relatively thick samples, where residual strain is not relieved by cutting into thin slices required for more traditional methods, such as X-ray diffraction. It has been demonstrated that thermal and cold neutron radiography is well suited for the investigation of macroscopic internal defects, as well as the distribution of impurities and voids [1]-[5]. With energy-resolved imaging it is possible to investigate some microstructure details within welds, such as the presence of large grains or preferred orientation within certain areas. The analysis of neutron

* To whom any correspondence should be addressed.

transmission spectra can provide information on the microstructure and enable studies of residual strain and texture-related characteristics within the sample. The sharp variation of neutron transmission at certain energies, the so-called Bragg edges, can be used for effective analysis of microstructure within the welds, as long as data is acquired with an adequate energy resolution. The conventional neutron diffraction techniques, already well established, provide data on phase, structure and microstructure, however with limited spatial resolution of a pencil beam scanned across the sample [6],[7]. Measurement of a neutron transmission spectrum in each pixel of the image has recently become available with relatively high spatial resolution of ~100 μm due to recent developments of high resolution neutron detectors capable of measuring both position and time for each detected particle [8], [9].

There are several options to achieve energy-resolution in neutron imaging. Due to the lack of high resolution energy-resolving neutron imaging detectors to this date, there have typically been at least two alternative approaches. 1. The incoming neutron flux is monochromatized by either a velocity selector or by a crystal monochromator and multiple images are measured by scanning through the energy range of interest. 2. Neutrons are produced in short pulses, and the energies of detected neutrons are measured via their time-of-flight. The energy resolution which can be achieved with a velocity selector is typically $dE/E \sim 15\%$ [10], which allows studies of texture variations and, to some extent, microstructure parameters such as crystallite size and orientation, but is not sufficient for the reconstruction of strain. The energy resolution of a double crystal monochromator setup is typically 3%, providing a higher energy resolution with the expense of neutron flux [11]. Recent developments of neutron imaging facilities at bright pulsed neutron sources [12], [13] enable studies with energy resolution $dE/E < 0.5\%$ [1], [14], [15] enabling mapping of the strain distributions with sub-mm spatial and ~100 microstrain resolution [16]. The unique combination of bright short-pulse neutron sources and high resolution neutron counting detectors, such as the neutron-sensitive MCP/Timepix used here, enables simultaneous detection of >250000 spectra in one acquisition. In this paper we demonstrate the capabilities of energy-resolved neutron imaging for the studies of microstructures within two steel welds. The distribution of residual strain and some texture variation across the samples are reconstructed with sub-mm resolution by the analysis of measured transmission spectra. Two steel welds are studied with the energy resolved neutron imaging: a butt friction stir weld between two steel plates and a conventional weld between two steel pipes.

2. Experimental setup

The experiments on energy-resolved neutron imaging were conducted at two pulsed neutron beamline facilities: at Engin-X at the ISIS spallation neutron source, Rutherford Appleton Laboratory, UK (friction stir weld) and at the Noboru beamline at the Japanese Proton Accelerator Complex (J-PARC). In both setups we used a high resolution MCP/Timepix neutron counting detector capable of simultaneous detection into multiple neutron energy bins with sub-μs timing resolution and 55 μm spatial resolution [8], [9]. More than 250000 spectra were measured simultaneously by 512x512 pixels, in an array consisting of 2x2 Timepix readout chips mounted behind neutron-sensitive microchannel plates. The energy of each registered neutron was calculated from its time of flight over distances of 50.0 m and 14.17 m for the Engin-X and Noboru experiments, respectively. The set of images, each corresponding to a narrow range of energy (typically dE/E~0.05%) was recorded in each measurement with ~3000 energy slices over the thermal and cold ranges of neutron energy. The measurement time was ~2.5 hours and ~1.5 hours for the friction stir weld and the pipe weld, respectively. It should be noted that the power of the J-PARC source was 200 kW during the latter measurement. However, with a planned increase of power to 1 MW the acquisition time will likely to be reduced to 20-30 minutes for similar neutron counting statistics. The measured spectra were normalized against spectra obtained when there was no sample in the beam. The latter normalization eliminated the effects of the beam spectrum anomalies including beam non-uniformities across the field of view. The samples were mounted at a distance of ~12 mm from the active plane of the detector. The beam divergence was defined by a set of slits and was less than 0.3°, thus limiting the image blur to ~1 pixel of our readout (55x55 μm^2). The active area of the detector used in these experiments was 28 mm in diameter. Multiple readouts per

single neutron pulse were implemented in the experiments in order to avoid event pileup. The readout time (limited by our detector deadtime) was 320 μs, resulting in the presence of small gaps in the measured spectrum which were chosen to be away from Bragg edges. Transmission along only one orientation of the sample was measured in the present experiments: for the friction stir weld, it was along the direction of the weld; and for the pipe weld, it was perpendicular to the axis of the pipe. The residual strain was measured as an integral over the entire thickness of the sample. The strain was reconstructed for each pixel of the measured data by fitting an analytical function into the measured Bragg edge transmission [15]-[18].

3. Results and discussion

3.1. Friction stir weld

A butt friction stir weld (FSW) between two 12.7 mm-thick chromium steel plates was characterized with the energy-resolved neutron transmission analysis. The steel composition (in wt %) was 10.5-12.5% Cr, 1.5% Mn, 0.3-1% Ni, 0.03% C, with small quantities of N, P, S and Si, and Fe balance. FSW welds were made at TWI (The Welding Institute, Abington, Cambridge, UK) using refractory metal welding tools of Whorl^{TM} type [19]. Shoulder diameter of 45mm was used with 10-14 mm probe diameter base-tip. During welding the plates were placed on a stainless steel bed and subjected to the down-force of 32 kN. The welding tool was advanced at the rotational speed of 625 r/min and lateral speed of 2mm/s. The dimensions of the completed welds were 203.2×66.2×12.7 mm^3. Infrared thermal imaging was used to monitor the temperature during welding, and revealed that a maximum of ~1000°C. Given the thermal history, the steel phase composition within the weld can be estimated with the help of the Schaeffler diagram [20], revealing that ferrite transforms to austenite during friction-induced heating, and that upon cooling the conversion of ferrite to martensite takes place. A 3mm-thick section out of the same weld has been studied previously by neutron diffraction at FRMII neutron source (Garching, Germany) [21]. However, for the purposes of stress analysis only BCC ferrite peak was used. In the present experiment it was possible to visualise the microstructure within an 11 mm-thick section of the weld (figure 1) using transmission neutron imaging. The contrast formation mechanism can be ascribed to the combination of phase composition and lattice structure, texture (preferred orientation) and residual strain.

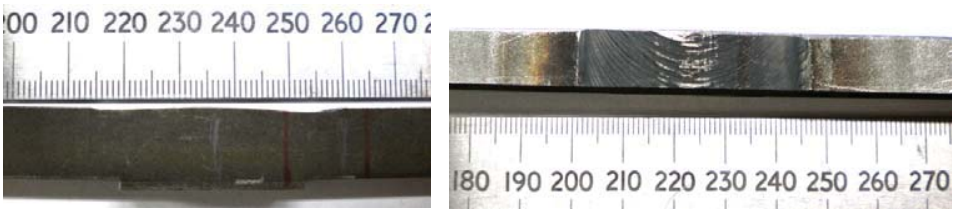

Figure 1. Photograph of the stir-friction weld characterised in the experiment. Left: view on the weld in the direction of neutron flux (longitudinal - direction of welding); Right – top view of the weld (normal direction to the surface of the plate).

The white-spectrum transmission image of the weld showed no features and looked similar to the image of figure 2.f at 4.19 Å. This image has a particular relevance because the wavelengths used in that image are just above the first (110) Bragg edge of BCC steel. It displays no structural features, as Bragg diffraction does not occur at these long wavelengths for BCC steel. The possibility to measure narrow-energy transmission is crucial for studies of phase, crystal and microstructure properties revealed by diffraction of neutrons out of the incident beam. The weld region is clearly seen in the images of figure 2, as well as the parent steel section with horizontal banding corresponding to a variation of texture within the plate due to the rolling manufacturing process.

The neutron transmission spectra obtained in different areas of the weld shown in figure 3 indicate the presence of strong texture within the original steel plates. The images of figure 2, at the same time, reveal the sizes of the textured layers within the plate, while the re-melted weld region shows some large-scale features only around the 110 Bragg edge at 4.06 Å (figure 2.e). The difference between the weld area and the original steel plate is demonstrated in figure 4. A quantitative analysis can be performed by fitting an analytical function to the measured Bragg edges [15]-[18]. Figure 5 illustrates the four fit parameters, which are affected by the microstructure within a sample. The position of the Bragg edge center can be determined with ~10 times better accuracy by fitting, compared to the measured width of the edge, which cannot be smaller than the wavelength resolution of the experimental setup (~0.5% in our case). By fitting the analytical function, the accuracy of strain reconstruction can be improved to a level of ~100 microstrain, depending on the neutron counting statistics in each small area of the sample, down to a single 55 µm pixel.

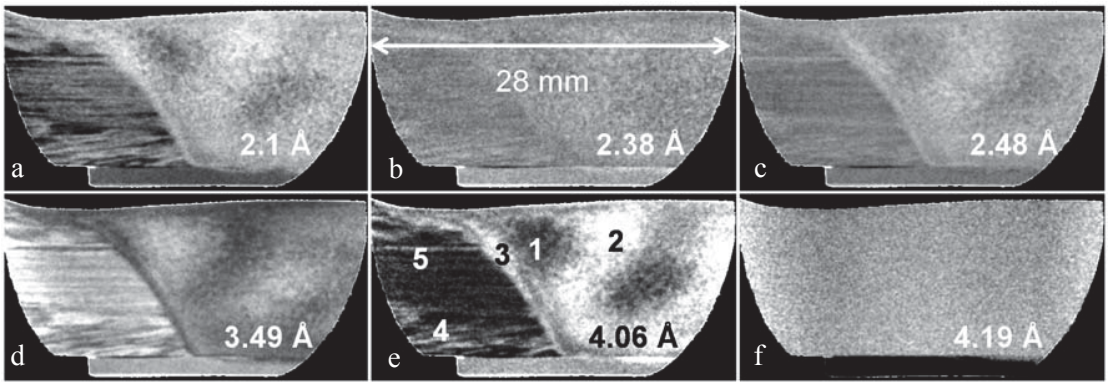

Figure 2. Narrow-energy neutron transmission images of the friction stir weld. The corresponding wavelength of each image is indicated. The labels 1-5 on the4.06 Å image indicate the areas for which spectra are plotted in figure 3.

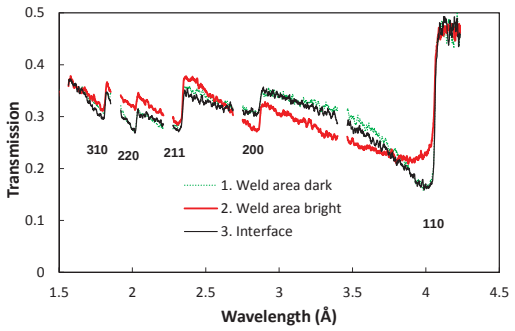

Figure 3.a. The measured transmission spectra of the weld in the areas within the heat affected zone, indicated by the numbers in figure 2.

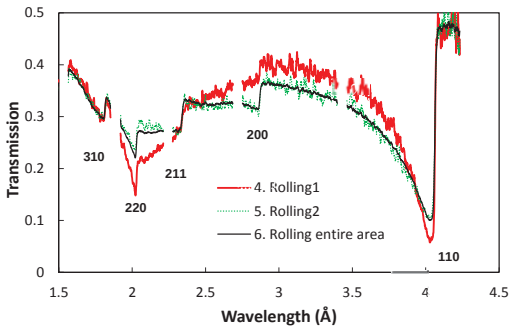

Figure 3.b. Same as figure 3.a, except measured for the areas outside of the weld. Spectra are characterised by strong texture of the rolled material.

The fitting results for the friction stir weld are shown in figures 6-11. The distribution of the residual strain across the sample was calculated from the spectra accumulated over a 1.1x1.1 mm^2 area around each 55 µm pixel, as indicated by the scale bar in figure 6. The '$\lambda_0=2d_0$'-reference value of 4.0534 Å for the strain calculation was taken from data collected in the stirred area of the weld, as demonstrated by the X-ray strain measurements performed on a thin section of the weld [21]. Even after the sample

was cut and major macroscopic stresses were nearly relived in the dominant direction (longitudinal) of the welding, the distribution profile can be seen with very high spatial resolution. Tensile strain values are measured in the area adjacent to the stirred zone in the direction along the weld seam. The width of the (110) Bragg edge is larger in the heat affected zone, as seen from figure 7, corresponding to a lower height of the edge, while the (211) edge height is higher in the heat affected zone as seen in figures 4 and 10. The images of figure 2 and spectra of figures 3 and 4 indicate that the rolling texture observed in the original steel plate is reduced in the heat affected region of the weld, while the residual strain distribution of figure 6 shows much lower strain values in the weld region compared to the adjacent area.

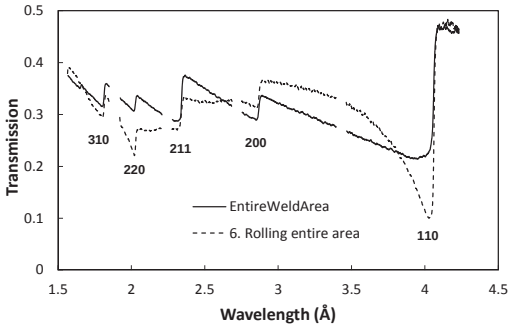

Figure 4. Same as figure 3.a, except shown for the entire weld and entire original steel pate areas.

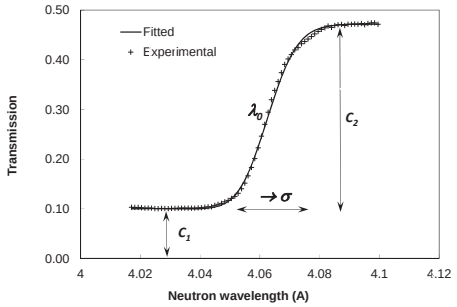

Figure 5. The 110 Bragg edge of measured transmission for the friction stir weld (markers) and the fitted analytical function.

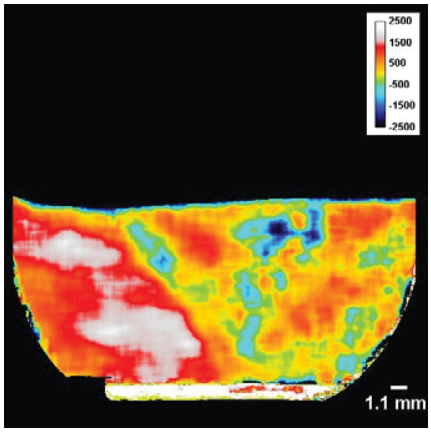

Figure 6. Strain reconstructed from 110 Bragg edge. The legend indicates strain values (με).

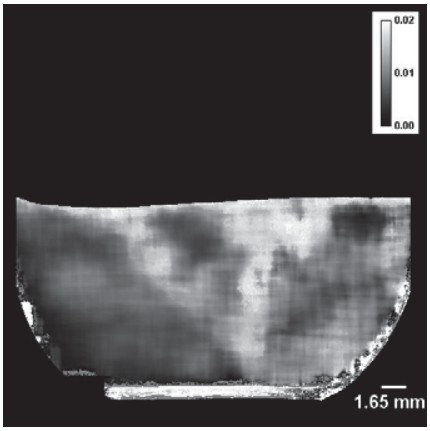

Figure 7. The width of the (110) Bragg edge, reconstructed by a fit to the experimental data.

3.2. Steel pipe weld

A weld between two FCC steel pipes with ~2.5 mm thick walls (figure 12) was investigated by energy resolved imaging at the J-PARC pulsed source facility. The sample was mounted with the incident beam direction perpendicular to the axis of the pipe, as shown in figure 12. The strain values integrated along the beam direction are shown in figure 13.a, with spectra taken in the 1.1x1.1 mm^2 area around each pixel. Different from the friction stir weld described in the previous section higher residual strains are concentrated around the seam area of the welded pipe. The '$\lambda_0=2d_0$'-reference value of 4.1486 Å for the strain calculation was taken as an average value from data collected at a distance from the weld. The

height and the pedestal of the Bragg edge shown in figures 13.b and 13.c indicate the presence of large grain orientation variations within the weld region. The narrow-energy band transmission images shown in figure 14 reveal the presence of highly textured areas within the weld, with needle-like structures of ~100 μm thickness. In addition to improved spatial resolution as compared to previously published images of similar welds [2], the improved energy resolution of our experimental setup enables measurements of the transmission spectra within small effective pixel sizes across the entire sample. The transmission spectra shown in figure 15 reflect the presence of the FCC polycrystalline steel structure in the area of the pipe not affected by welding, albeit with indications of considerable preferred orientation (see for example (111) Bragg edge shape of areas 1 and 2). In the region of the weld the spectra reveal the presence of microcrystallites, evidenced by pronounced dips rather than Bragg edges. These dips originating from a group of crystals coexist with the (111) Bragg edge (figure 15.b), indicating the presence of both a random-orientation polycrystalline component and a group of re-solidified large grains within the weld seam.

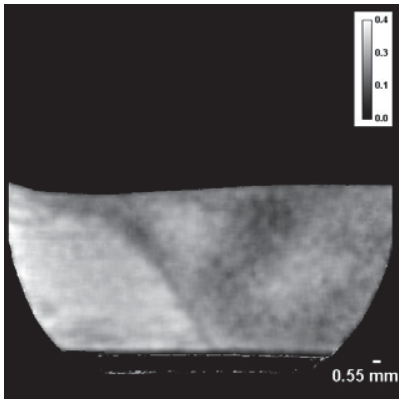

Figure 8. The distribution of height of the (110) Bragg edge (parameter C_2 of figure 5).

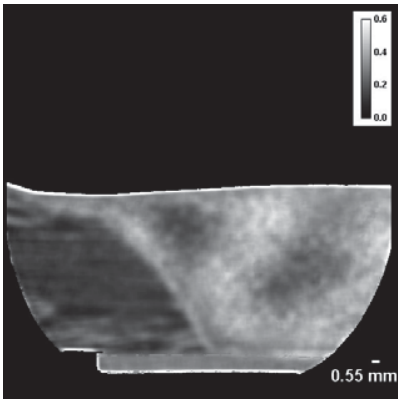

Figure 9. The distribution of (110) Bragg edge pedestal (parameter C_1 shown in figure 5).

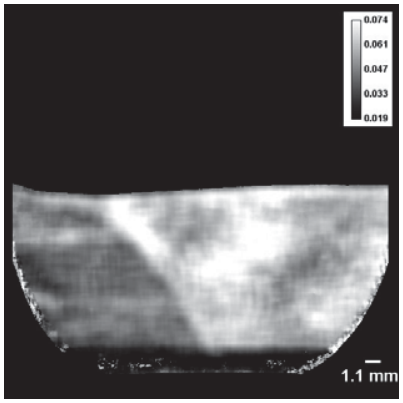

Figure 10. Same as figure 8, except for (211) Bragg edge.

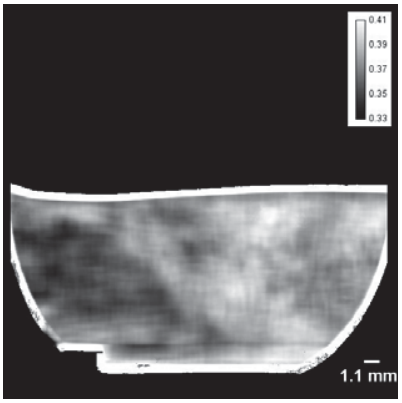

Figure 11. Same as figure 9, except for the (211) Bragg edge.

4. Conclusions

The recent development of bright pulsed neutron sources in combination with high resolution fast neutron counting detectors, enables improved studies of microstructures within weld samples, where strain and texture-related features can be mapped with ~100 μm spatial resolution. The simultaneous measurement of a spectrum in each 55x55 μm^2 pixel provides the potential of recovering some

quantitative information on the microstructure through Bragg edge analysis. More advanced Rietveld-type transmission spectrum analysis tools [22] enable mapping of various microstructure characteristics of the welds, throughout their bulk volume, and not merely on the surface. Although the analysis presented in this paper does not provide quantitative information on the orientation distribution function within the sample, as can be obtained with conventional neutron diffraction, the sequence of narrow energy-band images can nevertheless provide valuable and very quick complementary information on residual strain as well as uniformity of texture - with relatively high spatial resolution across the entire sample. It is advantageous that the full region of interest of a sample can be mapped using only a single measurement step, both spatially and as a function of energy.

Figure 12. Photograph of the steel pipe weld used in the experiment.

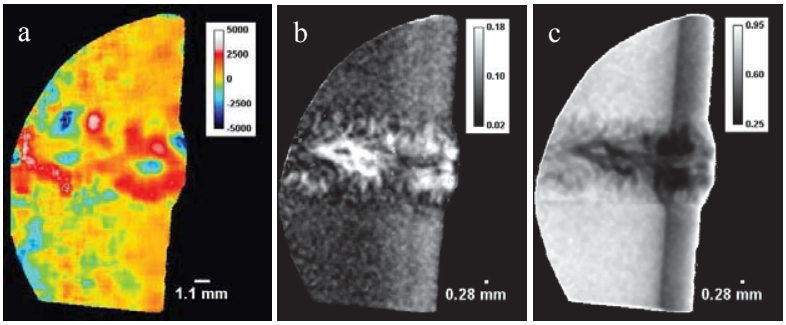

Figure 13. (a) Residual strain distribution obtained from measured spectra around (111) Bragg edge. (b) Height C_2 of the (111) Bragg edge. (c) Pedestal C_1 of the (111) Bragg edge.

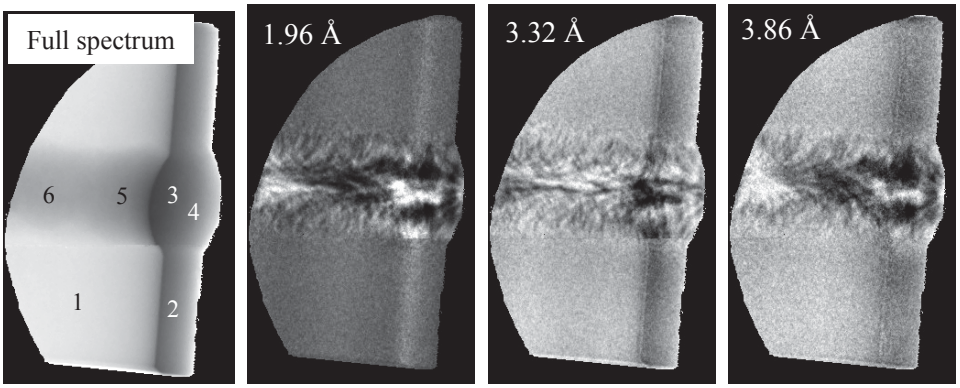

Figure 14. White beam spectrum image and narrow-energy-band images of the pipe weld.

Acknowledgments
The detector used in these experiments was developed within the Medipix collaboration. This work was supported in part by the U.S. Department of Energy under Grants No. DE-FG02-07ER86322, DE-FG02-08ER86353 and DE-SC0009657. The authors would like to acknowledge the generous donation of Vertex FPGA, Vivado design suite and DK-K7-CONN-G connectivity kit by Xilinx Inc. of San Jose, California through their Xilinx University Program.

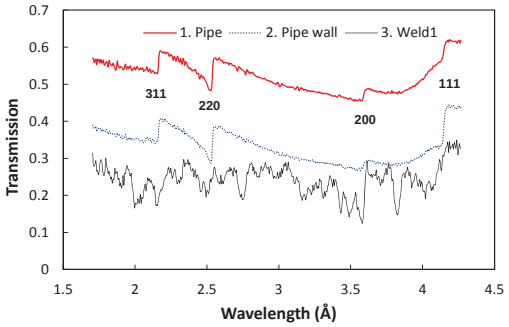

Figure 15.a. The measured transmission spectra of the pipe weld in the areas indicated by the numbers in figure 14.

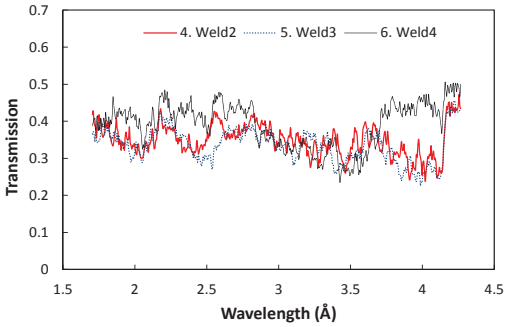

Figure 15.b. The measured transmission spectra of the pipe weld in the areas indicated by the numbers in figure 14.

References

[1] Kockelmann W, Frei G, Lehmann E H, Vontobel, P, Santisteban J R, Energy-selective neutron transmission imaging at a pulsed source, 2007. *Nucl, Instr, Meth. A* **578** 421.
[2] Lehmann E H, Frei G, Vontobel P, Josic L, Kardjilov N, Hilger A, Kockelmann W, Steuwer A., 2009. The energy-selective option in neutron imaging. *Nucl, Instr, Meth. A* **603** 429.
[3] Sato H, Kamiyama T, Iwase K, Ishigaki T, Kiyanagi Y., 2009. Pulsed neutron spectroscopic imaging for crystallographic texture and microstructure. *Nucl, Instr, Meth. A* **651** 216.
[4] Kardjilov N, Manke I, Hilger A, Williams S, Strobl M, Woracek R, Boin M, Lehmann E, Penumadu D, Banhart J, 2012. Neutron Bragg-edge mapping of weld seams. *Int. J. Mater. Res.* **103** 151.
[5] Santisteban J R, Vicente-Alvarez M A, Vizcaino P, Banchik A D, Vogel S C, Tremsin A S, Vallerga J V, McPhate J B, Lehmann E, Kockelmann W, 2012. Texture imaging of zirconium based components by total neutron cross-section experiments. *J. Nucl. Res.* **425** 218.
[6] Withers P J, Webster P J, 2001. Neutron and Synchrotron X-ray Strain Scanning. *Strain* **37** 19.
[7] Woo W, Feng Z, Wang X-L, David S A, 2011. Neutron Diffraction Measurements of Residual Stresses in Friction Stir Welding: A Review. *Sci. Tech. Welding and Joining* **16** 23.
[8] Tremsin A S, 2012. High resolution neutron counting detectors with microchannel plates and their applications in neutron radiography, diffraction and resonance absorption imaging. *Neutron News* **23** 35.
[9] Tremsin A S, Vallerga J V, McPhate J B, Siegmund O H W, 2015. Optimization of high count rate event counting detector with Microchannel Plates and quad Timepix readout. *Nucl, Instr, Meth. A* **787** 20.
[10] Wagner V, Friedrich H, Wille P, 1992. Performance of a high- tech neutron velocity selector *Phys. B: Cond. Matter* **180-181** 938.
[11] Schulz M, Boeni P. Calzada E, Mühlbauer M, Schillinger B, 2009. Energy-dependent neutron imaging with a double crystal monochromator at the ANTARES facility at FRM II. *Nucl, Instr, Meth. A* **605** 33.
[12] Kockelmann W, Zhang S Y, Kelleher J F, Nightingale J B, Burca G, James J A, 2013. IMAT–a new imaging and diffraction instrument at ISIS. *Phys. Procedia* **43** 100.
[13] Harada M, Oikawa K, KasugaiY, Maekawa F, 2011. Shielding Design of a Neutron Beam Line "NOBORU" at JSNS/J-PARC. *Prog. Nucl. Sci. Technol.* **1** 94.
[14] Santisteban J R, Edwards L, Steuwer A, Withers P J, 2001. Time-of-flight neutron transmission diffraction. *J. Appl. Crystal.* **34** 289.
[15] Steuwer A, Santisteban J R, Withers P J, Edwards L, Fitzpatrick M, 2003. In situ determination of stresses from time-of-flight neutron transmission spectra. *J. Appl. Crystal.* **36** 1159.

[16] Tremsin A S, McPhate J B, Steuwer A, Kockelmann W, Paradowska A M, Kelleher J F, Vallerga J V, Siegmund O H W, Feller W B, 2012. High-resolution strain mapping through time-of-flight neutron transmission diffraction with a microchannel plate neutron counting detector. *Strain* **48** 296.
[17] Vogel, S. 2000 *Proc. Math.-Naturwissenschaftliche Fak*. Uni Kiel Kiel. 174.
[18] Santisteban, J R, Edwards L, Fizpatrick M E, Steuwer A, Withers P J, 2002. Engineering applications of Bragg-edge neutron transmission. *App. Phys. A* **74** S1433.
[19] Mishra R S, Ma Z Y, 2005. Friction stir welding and processing. *Mater. Sci. Engn. Reports* **50** 1.
[20] Schaeffler A L, 1949. Constitution diagram for stainless steel weld metal. Metal Prog. **56(11)** 680.
[21] Jun T S, Hofmann F, Hofmann M, Korsunsky A M, 2009, Residual stress characterization in 12%-Cr steel friction stir welds by neutron diffraction. *J. Strain Anal*. **47** 204.
[22] Sato H, Kamiyama T, Kiyanagi Y, 2011. A Rietveld-Type Analysis Code for Pulsed Neutron Bragg-Edge Transmission Imaging and Quantitative Evaluation of Texture and Microstructure of a Welded α-Iron Plate. *Materials. Transactions* **52** 1294.